EXPERIMENTAL STUDY OF THERMAL ENERGY STORAGE RATES IN HIGH TEMPERATURE PHASE CHANGE SYSTEMS FOR SOLAR REFRIGERATION

Antoni Gil[1], Eduard Oró[1], Cristian Solé[1], Álvaro Ruiz[2], José Manuel Salmerón[2], Luisa F. Cabeza[1]

[1]GREA Innovació Concurrent, Universitat de Lleida, Edifici CREA, Pere de Cabrera s/n, 25001 Lleida, (Spain)
[2]Grupo de Termotecnia, Universidad de Sevilla, Edificio Escuela de Ingenieros, Camino de los Descubrimientos s/n, 41092 Sevilla, (Spain)

1. Introduction

High temperature thermal energy storage (TES) may play an important role in solar applications, becoming a key issue to increase the global effectiveness of this type of installations. Different sorts of thermal storage technologies in high temperature were reported in Gil et al. (2010). The key issue of TES systems is the selection of the best storage material for each application (Zalba et al., 2003; Medrano et al., 2010). The thermal properties of the material (basically the range of melting temperature and the enthalpy of phase change), the conservation of these properties after several thermal cycles, and possible corrosion problems with the container are some of the important aspects to take into account during the selection of the storage material. In order to test these characteristics experimental analysis with TES units are needed. Ait Adine et al. (2009) carried out a numerical analysis and experimental validation of the behavior of thermal properties of two phase change materials (PCM) in a shell-and-tube heat storage unit. The PCM were located around an only tube and their melting temperatures were 50 ºC and 27.7 ºC. This work assumed that the effect of natural convection during melting could be taken into account by using an effective thermal conductivity of the liquid phase of the PCM. This assumption will be taken in account too in the present work.

On the other hand, Bayon et al. (2010) studied the behaviour of the 54%wt KNO_3 / 46%wt $NaNO_3$ used as PCM in a shell-and-tubes storage tank. In this case the melting point of the material was 221 ºC. This work studied also the effective conductivity of the storage material during the melting process.

The aim of this paper is to study the behaviour of different PCM with similar melting temperature ranges (from 150 ºC to 200 ºC) as TES materials during the charging and discharging processes. Two different materials were selected and tested in the high temperature pilot plant of GREA at the University of Lleida. The first one was hydroquinone, which has a melting temperature range between 165 ºC and 173 ºC and a latent heat of 205.8 kJ/kg, and the second material tested was d-mannitol, which has a melting temperature range between 161 ºC and 170 ºC and a latent heat of 261.5 kJ/kg. Two identical high temperature storage tanks were designed and constructed in order to carry out the experimentation, to be able to compare both materials under the same boundary conditions. The results may help to understand the behaviour of the latent heat in the phase change, the power required in the melting process and the effective conductivity of the materials tested under different working conditions and the influence of these properties on the storage rates during charging processes.

2. Description of set-up

Two identical tanks were designed and constructed at the University of Lleida installations in order to evaluate the behavior of different high temperature PCM and to study their thermal properties during the melting process. The design was based on shell-and-tubes heat exchangers, where the heat transfer fluid (HTF) passes through the tubes and the PCM is located in the shell, between the tubes (Figure 1). The materials selected as PCM were hydroquinone and d-mannitol, with melting temperature ranges around 166-173 ºC and 161-170 ºC respectively, according to previous results obtained by DSC. The latent heat energy for these materials in these temperature ranges are 205.8 kJ/kg and 261.5 kJ/kg, respectively.

For a good analysis of the thermal behavior of the PCM, 27 temperature sensors were installed at different locations inside the tank. All the temperature sensors are Pt-100. Figure 2 shows the position of the different sensors installed in the TES tank. There are 15 sensors measuring the temperature of the PCM located

between the HTF tubes, in the body of the tank (TPCM.1 to TPCM.15). These sensors are distributed in 5 groups. Therefore each group has three sensors which had different length and are located at different height: the sensors in the bottom of the tank are 35 mm, 114 mm and 194 mm from the lateral wall, located in the bottom, middle and top of the tank respectively.

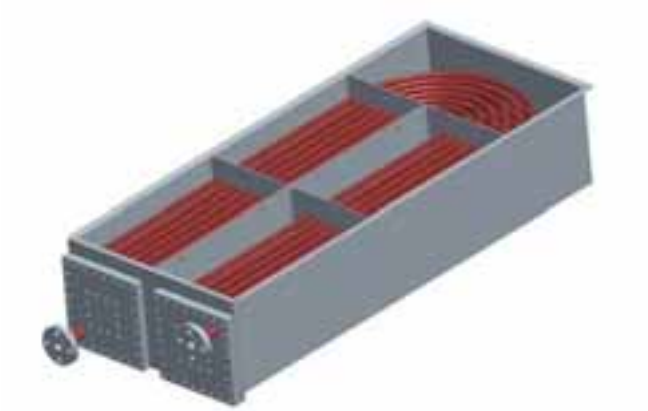

Figure 1. Storage tank design based on shell-and-tubes heat exchanger.

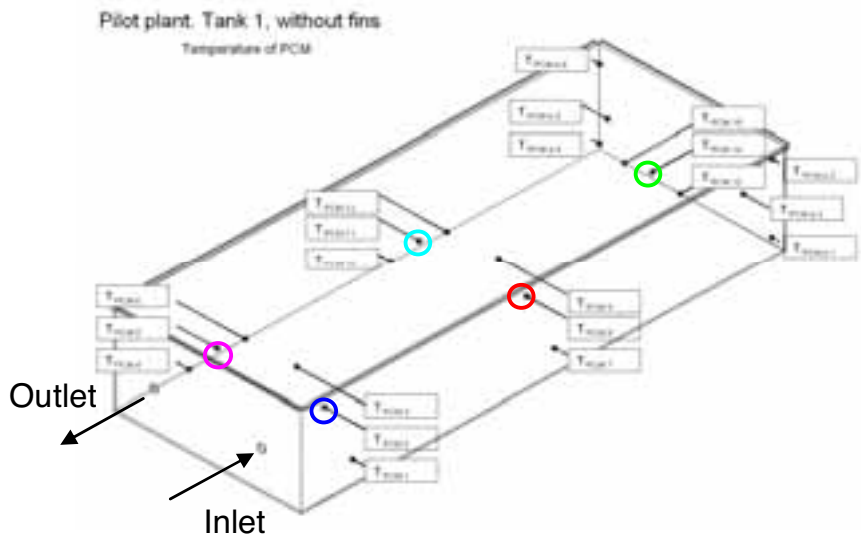

Figure 2. Location of the temperature sensors in the tank.

3. Methodology and calculations

Methodology of the experiments

The experiments (charge and discharge of PCM) were performed at two different temperature ranges, 130-200 ºC and 145-187 ºC, respectively. On the other hand, to encourage the characterisation of the process, three different HTF flow rates were used for each experiment, 1.4 m^3/h, 2.2 m^3/h and 3.0 m^3/h. Before every experiment the PCM temperature was set at the starting experiment temperature (130 ºC or 145 ºC, respectively). When the PCM temperature was homogeneous, the HTF temperature was increased up to the maximum temperature of the experiment (200 ºC or 187 ºC, respectively) outside the storage tank. Then, the HTF was driven through the tank.

In order to get an idea of the general temperature of the tank, the temperature sensors located at the middle part of it (TPCM.2, TPCM.5, TPCM.8, TPCM.11 and TPCM.14, as Figure 2 shows) were considered, taking as reference the value of the sensor TPCM.8 because it shows the more representative behavior of the PCM. The temperature range of melting and the melting period (interval time of melting) of hydroquinone and d-mannitol was determined thanks to the melting curve obtained in each experiment.

Effective conductivity calculations

The period while the melting process of the PCM takes place is the considered steady-state period. On the other hand, the effect of natural convection during the melting process is taken into account by using an effective thermal conductivity of the PCM liquid phase (Ait Adine et al., 2009).

In order to evaluate the effective conductivity of the PCM during the melting process, a diameter of maximum melting zone is defined ($D_{melting}$). This diameter corresponds to the distance between heat exchanger pipes and is the maximum heat flux influence zone. This assumption is good enough as a first approximation, but it neglects the amount of PCM located between $D_{melting}$ and $\sqrt{2} \cdot D_{melting}$.

These three assumptions allow calculating the effective conductivity of the PCM as shown in eq. 1 to eq. 5.

$$\dot{q} = \dot{m} \cdot \rho_{HTF} \cdot \bar{c}_{p|HTF} \cdot \Delta T_{HTF} = U \cdot A \cdot \Delta T_{lm} \quad \text{(eq. 1)}$$

$$\Delta T_{HTF} = T_{HTF,out} - T_{HTF,in} \quad \text{(eq. 2)}$$

$$U = \frac{1}{R_{HTF} + R_{tube} + R_{PCM}} = \frac{1}{\frac{D_{ext}}{h_{HTF} \cdot D_{\text{int}}} + \frac{D_{ext}}{2k_{tube}} \cdot \ln\left(\frac{D_{ext}}{D_{\text{int}}}\right) + \frac{D_{melting}}{2k_{effective}} \cdot \ln\left(\frac{D_{melting}}{D_{ext}}\right)} \quad \text{(eq. 3)}$$

$$A = \pi \cdot D_{ext} \cdot L \quad \text{(eq. 4)}$$

$$\Delta T_{lm} = \frac{\left(T_{HTF,in} - \overline{T}_{PCM}\right) - \left(T_{HTF,out} - \overline{T}_{PCM}\right)}{\ln\left(\frac{T_{HTF,in} - \overline{T}_{PCM}}{T_{HTF,out} - \overline{T}_{PCM}}\right)} \quad \text{(eq. 5)}$$

In the eq. 5 it was considered the average temperature of the melting range of temperature obtained experimentally.

Replacing eq. 2, eq. 3, eq. 4 and eq. 5 in eq. 1, the effective conductivity can be determined.

Because the amount of PCM is not the same in the two tanks and in order to compare the melting processes of the materials, a ratio power/mass is defined. This ratio establishes the power involved in the melting process per kg of PCM. The power considered is the average power supplied by the HTF to the PCM during the melting process. This power is divided by the corresponding amount of PCM in each tank.

4. Results and discussion

The melting interval time of the PCM depends basically on the power supplied by the HTF. Therefore, expected results should show a decrease of the melting interval time with the increase of the temperature range and with the increase of the flow rate. In this paper, only the melting process of the experiments carried out with a flow rate of 3.0 m^3/h are shown.

Figure 3 and Figure 4 show the hydroquinone results. Comparing these results it may be seen that in the experiment with temperature range of 145-187 ºC the melting process is longer than in the experiment with range of 130-200 ºC. According to the temperature range observed during the experiments a melting interval time can be defined. In Figure 3 the melting curve of hydroquinone changes its slope showing very clearly the melting period. In Figure 4 the melting curve does not shows this slope change because the energy supplied by the HTF is higher. That leads to faster and inhomogeneous PCM melting in the tank. Table 1 shows that the melting interval decreases with the increase of the experiment temperature range. It is important to point out that the melting process occurs approximately at the melting range obtained by DSC (168-173 ºC).

Figure 5 and Figure 6 show the d-mannitol results during its melting process. The same effect described for the hydroquinone may be seen: the change in slope of the melting curve and the homogeneity of the melting process for the lower temperature range (145-187 ºC) are clearer. It may be observed that the melting interval of d-mannitol for the temperature range between 130-200 ºC decreased heavily.

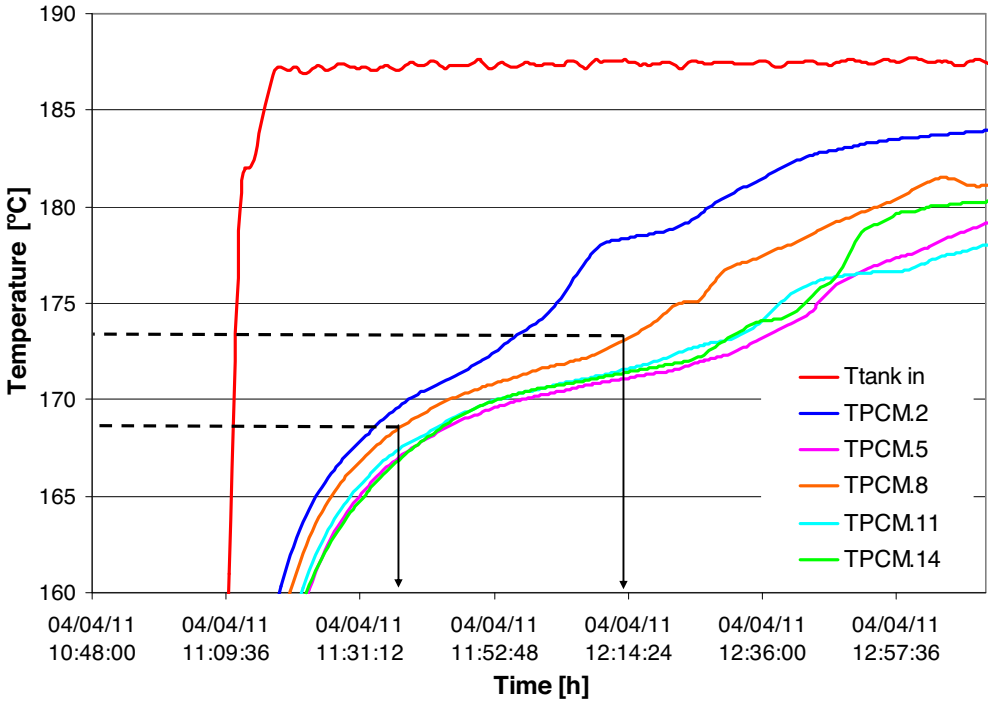

Figure 3. Hydroquinone results, melting temperature range 145-187 ºC, flow rate 3 m^3/h.

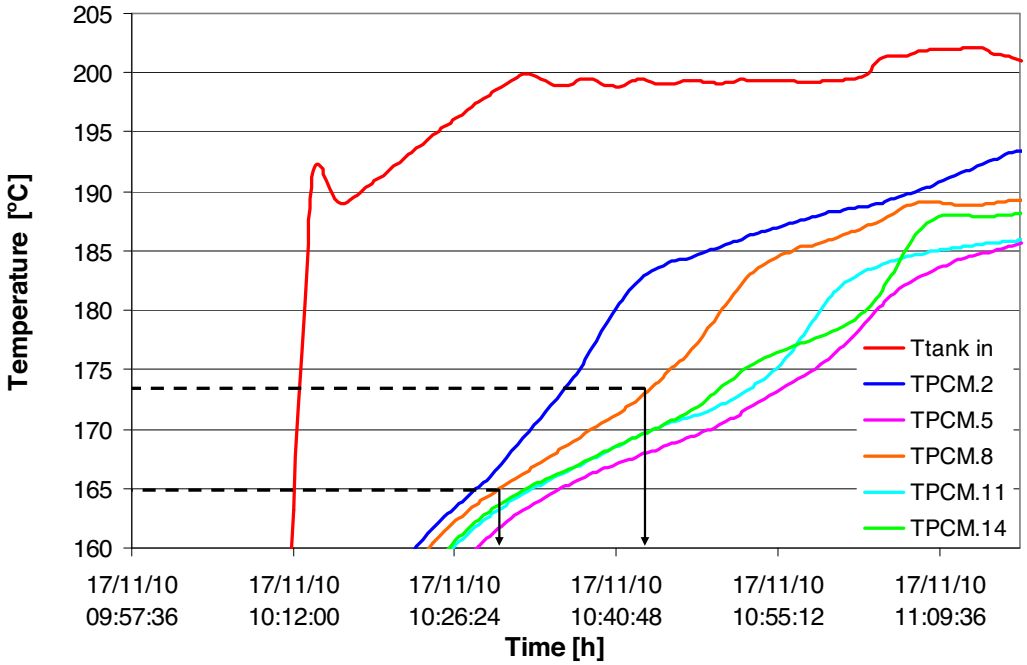

Figure 4. Hydroquinone results, melting temperature range 130-200 ºC, flow rate 3 m^3/h.

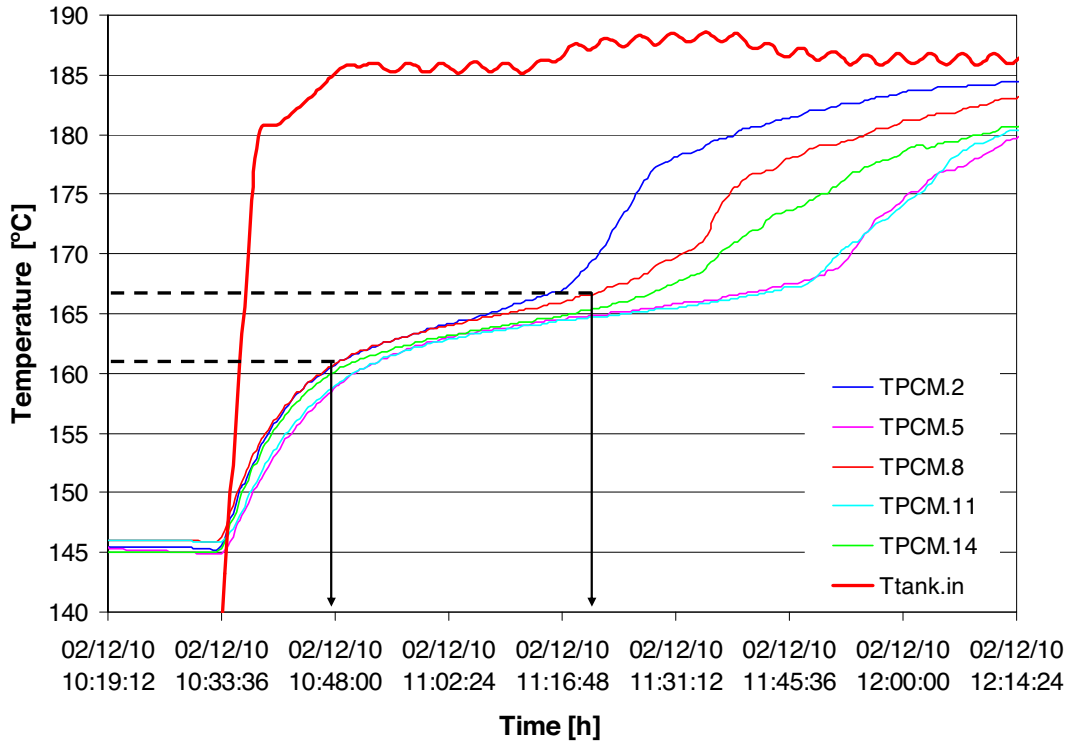

Figure 5. d-Mannitol results, melting temperature range 145-187 ºC, flow rate 3 m^3/h.

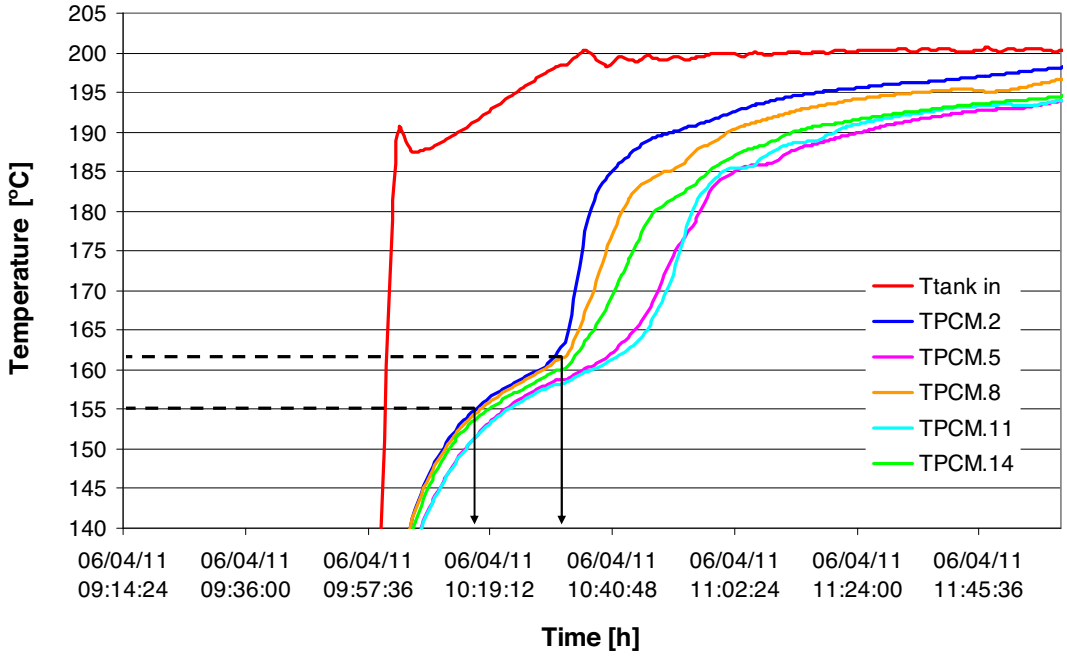

Figure 6. d-Mannitol results, melting temperature range 130-200 ºC, flow rate 3 m^3/h.

As in the case of hydroquinone, Table 1 shows that the melting interval decreases with an increase of the temperature range. Table 1 also shows that the d-mannitol melting process for the experimentation temperature range of 145-187 ºC takes place between 160 and 168 ºC, while for the temperature range of 130-200 ºC it is between 155 and 165 ºC. This difference could be caused by changes on thermal properties of d-mannitol.

Table 1. PCM melting intervals for each experiment.

Flow rate	Hydroquinone (145-187 ºC)	Hydroquinone (130-200 ºC)	d-Mannitol (145-187 ºC)	d-Mannitol (130-200 ºC)
1.4 m^3/h	57 min (168-174 ºC)	27 min (168-172 ºC)	63 min (161-168 ºC)	30 min (155-165 ºC)
2.2 m^3/h	47 min (168-173 ºC)	14 min (165-173 ºC)	45 min (161-168 ºC)	17 min (156-163 ºC)
3.0 m^3/h	37 min (168-173 ºC)	12 min (165-173 ºC)	39 min (160-167 ºC)	16 min (156-162 ºC)

However comparing the results of the two PCM studied, the results from d-mannitol shows that its melting period is longer than the one from hydroquinone because the enthalpy of d-mannitol is higher than the hydroquinone one.

Table 2 shows the power/mass of PCM ratio obtained for every experiment. The ratio power/mass of PCM increases with the flow rate and temperature ranges because the power supplied increases. On the other hand, due to the higher melting enthalpy of the d-mannitol compared to hydroquinone the ratios power/mass of PCM obtained are higher for d-mannitol than for hydroquinone.

Table 2. Ratio power/mass of PCM for each experiment.

	Hydroquinone (145-187 ºC)	Hydroquinone (130-200 ºC)	d-Mannitol (145-187 ºC)	d-Mannitol (130-200 ºC)
1.4 m^3/h	0.026 kW/kg	0.046 kW/kg	0.040 kW/kg	0.068 kW/kg
2.2 m^3/h	0.032 kW/kg	0.062 kW/kg	0.050 kW/kg	0.081 kW/kg
3.0 m^3/h	0.035 kW/kg	0.077 kW/kg	0.058 kW/kg	0.096 kW/kg

Figure 7 shows melting period in function of the ratio power/mass of PCM. As it may be observed, an increase of the ratio power/mass of PCM leads to a decrease of the melting period.

It has been pointed out that the melting periods have a tendency of a minimum near 12 minutes for the hydroquinone and 16 minutes for the d-mannitol.

Table 3 shows the effective conductivity of hydroquinone and d-mannitol for each experiment. The values are between 0.29 and 0.46 W/m·K.

Table 3. PCM effective conductivity in each experiment.

	Hydroquinone (145-187 ºC)	Hydroquinone (130-200 ºC)	d-Mannitol (145-187 ºC)	d-Mannitol (130-200 ºC)
1.4 m^3/h	0.294 W/m·K	0.346 W/m·K	0.367 W/m·K	0.339 W/m·K
2.2 m^3/h	0.303 W/m·K	0.372 W/m·K	0.416 W/m·K	0.426 W/m·K
3.0 m^3/h	0.335 W/m·K	0.461 W/m·K	0.461 W/m·K	0.451 W/m·K

Figure 8 shows the effective conductivity calculated for each experiment. The hydroquinone effective conductivity shows a trend: it increases with the power/mass of PCM ratio because natural convection of the liquid PCM obtained during the melting process is included in the conductivity. The d-mannitol effective conductivity is almost the same for the different temperature ranges evaluated. This irregular behavior on thermal properties could be a consequence of changes in the nature of the d-mannitol in the heating or cooling process. This effect is under study.

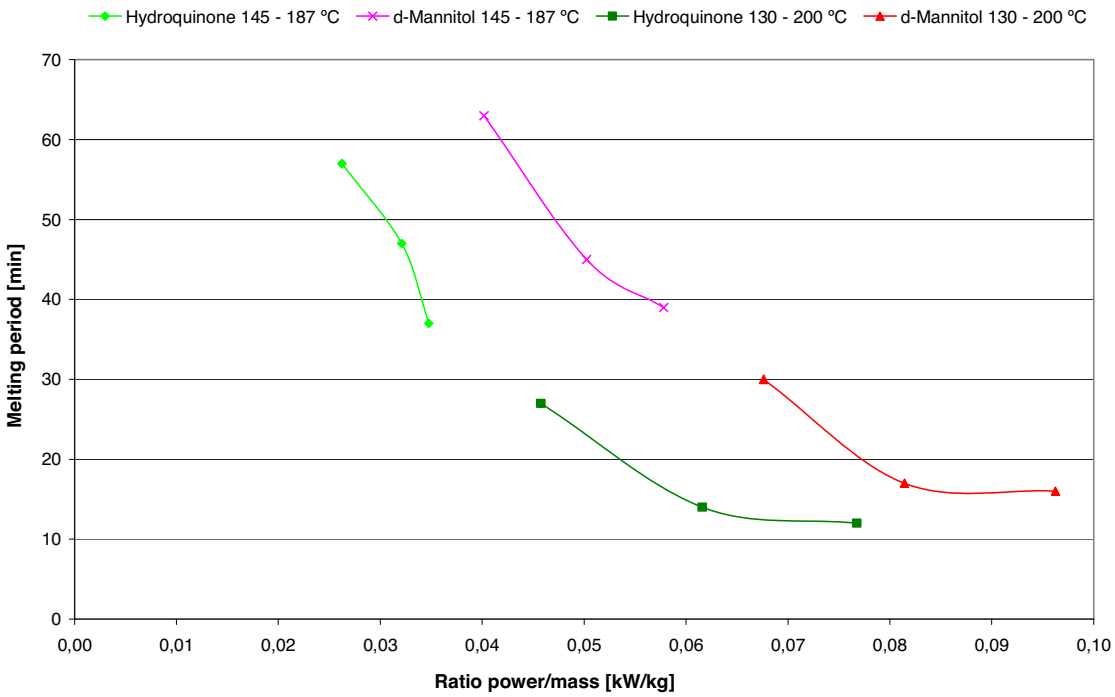

Figure 7. PMC melting period vs. ratio power/mass of PCM.

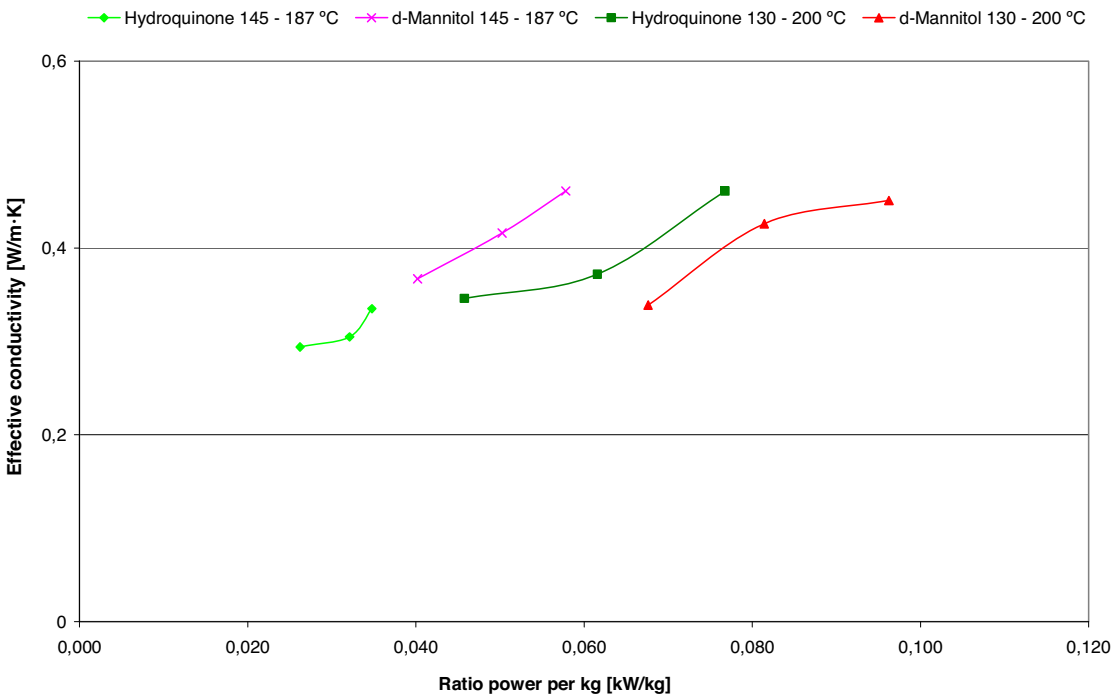

Figure 8. Effective conductivity in each experiment.

5. Conclusions

The experimental melting range of hydroquinone is around 165 ºC and 173 ºC as it was expected according the results obtained by DSC analysis. On the other hand, for d-mannitol the melting range is shorter than the expected one. Both melting ranges decrease when the ratio power/mass of PCM decrease.

The ratio power/mass of d-mannitol is higher than the hydroquinone one because the melting enthalpy of d-mannitol is also higher.

The effective conductivity of hydroquinone shows a tendency to increase with the ratio power/mass of PCM. The conductivity increases because the natural convection term is included in the calculations.

The d-mannitol melting range varies depending on the temperature range of the experiment and it disagrees with values obtained by DSC analysis. On the other hand, the effective conductivity trend of the d-mannitol is not constant. The causes of these effects are under investigation.

Finally, the effective conductivity varies between 0.294 and 0.461 W/m·K for hydroquinone, and beetween 0.367 and 0.461 W/m·K for d-mannitol.

6. Nomenclature

	Symbol	Unit
Diameter of maximum melting zone	$D_{melting}$	m
External diameter of the tank tubes	D_{ext}	m
Internal diameter of the tank tubes	D_{int}	m
Average length of the tank tubes	L	m
Surface of heat exchange	A	m^2
Heat flux	$\dot{Q}$	kW
Flow rate of HTF	$\dot{m}$	$m^3 \cdot s^{-1}$
Density of HTF	ρ_{HTF}	$kg \cdot m^{-3}$
Average specific heat of HTF	$\bar{c}_{p\|HTF}$	$J \cdot g^{-1} \cdot K^{-1}$
Difference of HTF inlet and outlet temperature	ΔT_{HTF}	ºC
Inlet temperature of HTF	$T_{HTF,in}$	ºC
Outlet temperature of HTF	$T_{HTF,out}$	ºC
Average melting temperature of the PCM	T_{PCM}	ºC
Overall heat transfer coefficient	U	$W \cdot m^{-1} \cdot K^{-1}$
Thermal resistance of the HTF	R_{HTF}	$M \cdot K \cdot W^{-1}$
Thermal resistance of the tube	R_{tube}	$m \cdot K \cdot W^{-1}$
Thermal resistance of the PCM	R_{PCM}	$M \cdot K \cdot W^{-1}$
Coefficient of heat transmission of the HTF	h_{HTF}	$W \cdot m^{-1} \cdot K^{-1}$
Conductivity of the tube material	k_{tube}	$W \cdot m^{-2} \cdot K^{-1}$
Effective conductivity of PCM	k_{PCM}	$W \cdot m^{-2} \cdot K^{-1}$

7. Acknowledgements

The work was partially funded by the Spanish government (project ENE2008-06687-C02-01/CON). The authors at GREA-UdL would like to thank the Catalan Government for the quality accreditation given to their research group (2009 SGR 534) and to Gas Natural by their support. Antoni Gil would like to thank the Col·legi d'Enginyers Industrials de Catalunya for his research appointment and the Departament d'Universitats, Recerca i Societat de la Informació of Generalitat de Catalunya for the AGAUR research stage scolarship (BE-DGR 2010).

8. References

Ait Adine, H., El Qarnia, H., 2009. Numerical analysis of the thermal behavior of a shell-and-tube heat storage unit using phase change materials. Applied mathematical modelling, Vol 33, 2132-2144.

Bayón, R. Rojas, E., Valenzuela, L., Zarza, E., León, J., 2010. Analysis of the experimental behaviour of a 100 kWth latent heat storage system for direct steam generation in solar thermal power plants. Applied thermal engineering, Vol 3, 2643-2651.

Gil, A., Medrano, M., Martorell, I., Lázaro, A., Dolado, P., Zalba, B., Cabeza, L.F., 2010. State of the art on high temperature thermal energy storage for power generation. Part 1-Concepts, materials and modellization. Renewable and Sustainable Energy Reviews, Vol 14, 31-55.

Medrano, M., Gil, A., Martorell, I., Potau, X., Cabeza, L.F., 2010. State of the art on high-temperature thermal energy storage for power generation. Part 2-Case studies. Renewable and Sustainable Energy Reviews, Vol 14, 56-72.

Zalba, B., Marin, J.M., Cabeza, L.F., Mehling, 2003. H., Review on thermal energy storage with phase change: Materials, heat transfer analysis and applications. Applied Thermal Engineering, Vol 23, 251-283.